Characterization of the Monomeric Form of the Transmembrane and Cytoplasmic Domains of the Integrin β3 Subunit by NMR Spectroscopy†

Renhao Li,‡ Charles R. Babu,‡ Kathleen Valentine,‡ James D. Lear,‡ A. Joshua Wand,‡ Joel S. Bennett,*,§ and William F. DeGrado*,‡

Department of Biochemistry and Biophysics, Johnson Research Foundation, and Hematology−Oncology Division, Department of Medicine, University of Pennsylvania School of Medicine, Philadelphia, Pennsylvania 19104

Received September 9, 2002; Revised Manuscript Received November 5, 2002

ABSTRACT: We have characterized a membrane protein containing residues P688−T762 of the integrin β3 subunit, encompassing its transmembrane and cytoplasmic domains, by nuclear magnetic resonance spectroscopy. Under conditions in which it is monomeric in dodecylphosphocholine micelles, the protein consists mainly of α-helical structures. An amino-terminal helix corresponding to the β3 transmembrane helix extends into the membrane-proximal region of the cytoplasmic domain. Moreover, following an apparent hinge at residues H722−D723, residues K725−A735 are mostly α-helical. In the presence of membrane-mimicking detergents, the cytoplasmic domain connected to the transmembrane helix is substantially ordered at pH 4.8 and 50 °C. Its carboxyl-terminal end takes on a turn−helix configuration characteristic of the immunoreceptor tyrosine-based activation motif. These structural features of the β3 subunit should help to explain its interaction with numerous cytosolic interacting proteins and begin to illuminate the mechanism of integrin activation.

Integrins, a superfamily of cell adhesion receptors, are critically involved in cell−cell adhesion and cell−matrix interactions (*1*). Moreover, by serving as signaling conduits across the membrane, they are involved in biological processes such as cell migration and malignant transformation (*1*). Each integrin consists of an α and a β subunit, both of which contain a large amino-terminal extracellular domain, a single transmembrane domain, and a short cytoplasmic tail. Integrin extracellular domains interact with extracellular macromolecular ligands. Recently, the X-ray crystal structures of the extracellular domain of the integrin α$v\beta$3, alone (*2*) and bound to an RGD ligand (*3*), were reported.

On the basis of patterns of sequence conservation, the portion of the β subunit not included in the α$v\beta$3 crystal structure is thought to consist of a transmembrane domain and membrane-proximal and membrane-distal regions of the cytoplasmic domain (Figure 1). Recent experiments suggest that the β subunit transmembrane domain participates in a monomer−oligomer equilibrium that may be important for regulation of integrin activation states (*4*). Indeed, mutations that enhance β3 subunit oligomerization have been found to enhance the ability of the integrin α$IIb\beta$3 to bind soluble ligands (*5*). The membrane-proximal region of the cytoplasmic domain may also play a role in regulating integrin activity. This highly conserved region is preceded by a classical membrane interface WK motif although the following four to five consecutive hydrophobic residues appear to be buried in the membrane as assessed by glycosylation mapping (*6*). This region of the β subunit cytoplasmic domain may mediate the interaction of integrins with cytosolic proteins such as focal adhesion kinase or paxillin (*7*). Indeed, because this region has been proposed to be an extension of the transmembrane helix, it may be one component of a single structural unit for transducing conformational changes between the cytoplasmic and extracellular domains (*6*, *8*). The interface between the membrane-proximal and the membrane-distal regions of β subunit cytoplasmic tails is marked by a conserved HD dipeptide. The distal region can be further subdivided into three subdomains on the basis of sequence homology (*9*). Of particular interest is a region that contains an NPXY motif thought be involved in binding to the cytoskeletal protein talin (*10*).

Previous reports of the structure of soluble β3 cytoplasmic tail peptides indicate that it is largely unstructured in the absence of organic solvents such as trifluoroethanol (*11*−*13*), even when attached to a water-soluble coiled-coil construct (*14*). Nonetheless, two recent NMR[1] studies have suggested that the N-terminal portion of the β3 cytoplasmic tail, including the membrane-proximal region, is mostly α-helical when complexed with the membrane-proximal region of αIIb, although the details of the heterodimeric

† This work was supported by NIH Grants HL54500 (J.S.B. and W.F.D.) and DK39806 (A.J.W.). R.L. was supported in part by a postdoctoral fellowship from the Cancer Research Fund of the Damon Runyon-Walter Winchell Foundation (DRG-1536). C.R.B. was supported by an NIH postdoctoral fellowship (GM20806).

* To whom correspondence should be addressed. W.F.D.: tel, (215) 898-4590; fax, (215) 573-7229; e-mail, wdegrado@mail.med.upenn.edu. J.S.B.: tel, (215) 573-3280; fax, (215) 573-7039; e-mail, bennetts@mail.med.upenn.edu.

‡ Department of Biochemistry and Biophysics, Johnson Research Foundation, University of Pennsylvania.

§ Hematology−Oncology Division, Department of Medicine, University of Pennsylvania School of Medicine.

[1] Abbreviations: CD, circular dichroism; DPC, dodecylphosphocholine; NMR, nuclear magnetic resonance; NOE, nuclear Overhauser effect.

10.1021/bi026822l CCC: $22.00
Published on Web 12/10/2002

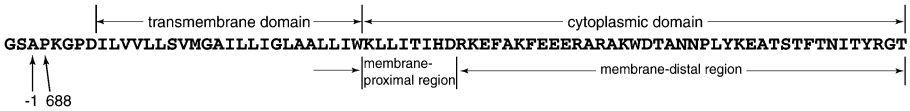

FIGURE 1: Amino acid sequence of the β3 TM-CYTO protein. The consensus transmembrane and cytoplasmic domains, as well as the membrane proximal and distal regions, are labeled. Except for the N-terminal three residues, the residues are numbered as in the full-length mature β3 subunit.

interaction depicted in these two studies differ substantially (*15*, *16*). On the other hand, two other NMR studies of peptides spanning the entire cytoplasmic domain or the transmembrane−cytoplasmic domains of the same proteins failed to demonstrate that these proteins interact (*4*, *14*). Moreover, when peptides corresponding to the αIIb and β3 cytoplasmic tail are dispersed into micelles, they do not interact (*16*).

We have synthesized a protein corresponding to the transmembrane and cytoplasmic domains of β3 (β3 TM-CYTO). CD spectroscopy of this protein, dispersed in DPC micelles, indicated that it contains substantial regions of α-helix (*4*). Here, we have characterized the monomeric form of this protein in DPC micelles using triple-resonance NMR spectroscopy. The transmembrane domain and the membrane-proximal region of the cytoplasmic tail form a single α-helix, providing a potential continuous trimerization site. Although the cytoplasmic tail is not in a unique and stable conformation, it is largely structured. In particular, two regions of the tail are predominantly α-helical, as indicated by local ^{1}H−^{1}H NOEs, chemical shifts, $^3J_{NH\alpha}$ coupling constants, and heteronuclear ^{15}N NOE values. The structured regions in the cytoplasmic tail correspond to the binding sites for a number of cytoplasmic and cytoskeletal proteins. Thus, these studies may provide a structural basis for β3 cytoplasmic tail-mediated cytoskeletal interactions and for associated downstream signaling.

MATERIALS AND METHODS

Proteins and Materials. The β3 TM-CYTO protein containing β3 residues P688 → T762, either unlabeled or isotope-enriched, was expressed, purified, and dispersed into DPC micelles as described earlier (*4*). DPC was purchased from Avanti Polar Lipids. Deuterated DPC, sodium acetate, and D_2O were from Cambridge Isotope Laboratories.

Analytical Ultracentrifugation. Equilibrium sedimentation was carried out in a Beckman XL-I analytical ultracentrifuge, largely as previously described (*4*). To eliminate the DPC contribution to the buoyant molecular weight, 56.1% D_2O was added to the buffer (10 mM DPC, 50 mM sodium acetate, 50 mM KCl, 1 mM $MgCl_2$, pH 4.80) at 20 °C; 49.1% D_2O was added to the same buffer at 30 °C and 45.4% D_2O at 40 °C. The molecular weights (adjusted for exchangeable amide protons) and partial specific volumes of the protein were 8744.4 Da and 0.7605 cm^3/g at 20 °C, 8735.7 Da and 0.7655 cm^3/g at 30 °C, and 8730.8 Da and 0.7702 cm^3/g at 40 °C. At each temperature, protein samples at three protein/DPC ratios (1/300, 1/500, and 1/700) were centrifuged at three different speeds to equilibrium. The absorption at 280 nm as a function of radius was monitored and analyzed by nonlinear least-squares global curve fitting (*4*). Finally, dissociation constants obtained at lower temperatures were extrapolated linearly in a van't Hoff plot to generate a dissociation constant at 50 °C.

CD Spectroscopy. Two buffer systems, a more physiological buffer (25 mM MOPS, 100 mM KCl, 1 mM $MgCl_2$, pH 7.40) and an NMR buffer (50 mM sodium acetate, 1 mM $MgCl_2$, pH 4.80), were used. Protein samples were dissolved in buffers containing 10 mM DPC to a final concentration of approximately 20 μM (i.e., a protein/DPC ratio of 1/500). All spectra were collected on an Aviv Associates 62A DS spectrometer with a scan speed of 10 nm/min, an averaging time of 4 s, and a bandwidth of 1.5 nm. Cuvettes of 0.1 and 0.02 cm were used for spectra collection. Six scans for each sample were recorded, averaged, and corrected for buffer contribution.

NMR Spectroscopy. For sample preparation, ^{13}C,^{15}N-labeled β3 TM-CYTO protein was mixed with deuterated DPC as described earlier (*4*). The protein−DPC mixture was then dissolved in 400 μL of freshly made NMR buffer (50 mM deuterated sodium acetate, 0.02% sodium azide, 1 mM $MgCl_2$, pH 4.80) and placed into a 5 mm microtube (Shigemi). The final protein and DPC concentrations were 0.9 and 500 mM, respectively. All NMR spectra were recorded at 50 °C on a Varian Inova spectrometer operating at 750 MHz (^{1}H). The protein was stable during NMR data collection at 50 °C as no precipitation was visible in the sample tube afterward and the ^{15}N-HSQC spectrum was unchanged during data collection.

For backbone assignments, ^{15}N-HSQC, ^{13}C-HSQC, HNCACB, CBCA(CO)NH, and HNCO experiments were performed (*17*−*20*). An ^{15}N-NOESY-HSQC spectrum (*21*) was collected with a mixing time of 125 ms. The {^{1}H}-^{15}N NOE (*22*) was recorded in an interleave manner with and without broad-band ^{1}H saturation and with a relaxation delay of 1.5 s and a saturation time of 5.0 s. To obtain the $^3J_{NH\alpha}$ coupling constants, the HNHA experiment (*23*) was performed with a delay period of 25 ms. The data were processed using NMRPipe (*24*) and analyzed with XEASY (*25*).

RESULTS

The β3 TM-CYTO protein, originally produced as a GST fusion protein, has 78 residues (Figure 1). The amino-terminal three residues, numbered from -3 to -1, are part of the thrombin cleavage site that follows GST. The remainder of the protein, numbered as in full-length β3, contains its complete transmembrane and cytoplasmic domains.

Oligomeric State of the β3 TM-CYTO Protein at pH 4.8 and 50 °C. Ideally, for NMR studies, only one oligomeric form of a protein should be present. In DPC micelles at room temperature, the β3 TM-CYTO protein exists in a monomer−trimer equilibrium (*4*). Thus, it was important to identify conditions in which the monomeric form is predominant (>95%).

Analytical ultracentrifugation was employed to characterize the oligomeric state of the β3 TM-CYTO protein at pH

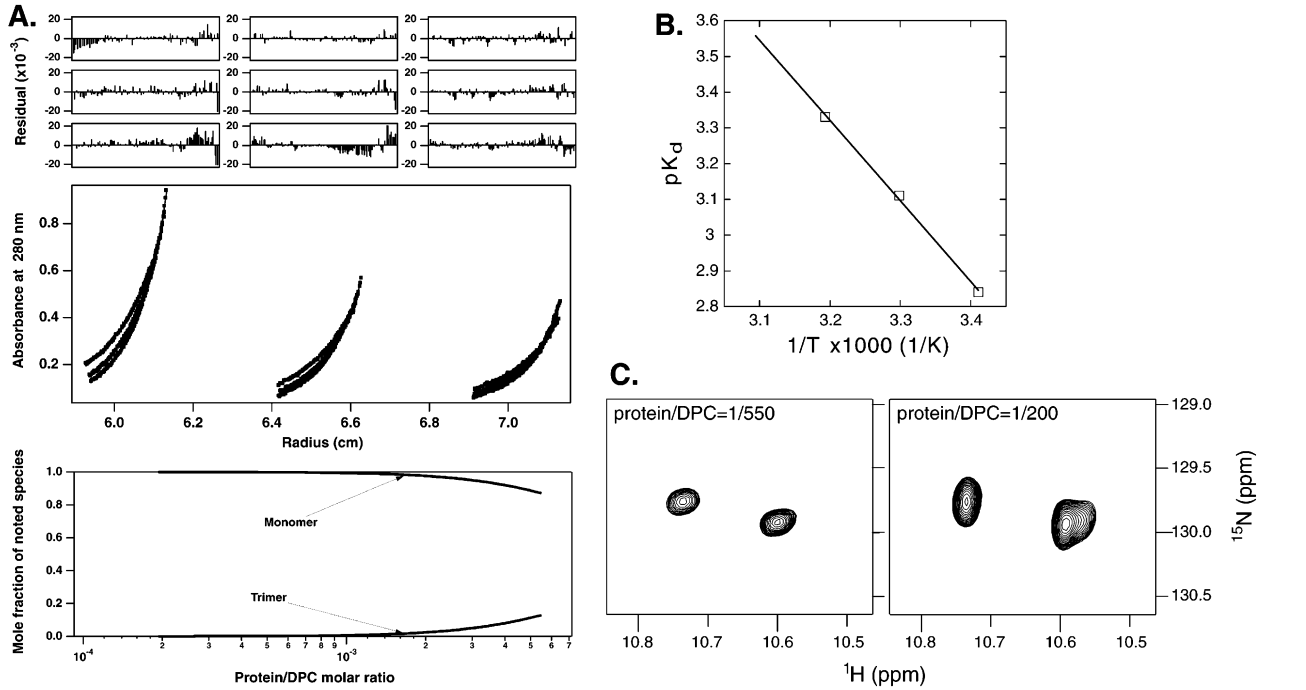

FIGURE 2: Characterizing the oligomeric state by analytical ultracentrifugation. (A) Equilibrium sedimentation of the β3 TM-CYTO protein at pH 4.8 and 40 °C. The central panel shows equilibrium A_{280} vs radius profiles for three samples of different peptide/detergent ratios (1/300, 1/500, and 1/700) at speeds of 40K, 45K, and 48K rpm. The lines represent the best fit to the data depicting a monomer−trimer equilibrium model. The top panels are residual plots. The bottom panel shows the plot of the calculated relative composition of different species versus the peptide/detergent molar fraction over the range observed in the experiments. The observed species are labeled in the plot. (B) van't Hoff plot depicting the temperature effect on homotrimerization of the β3 TM-CYTO protein in DPC micelles at pH 4.8. pK_d is the negative log of the dissociation constant of the monomer−trimer equilibrium expressed in mole fraction (peptide/detergent) units. (C) Comparison of the indole cross-peaks in ^{15}N-HSQC spectra at different protein/detergent ratios. The difference in line shape on the ^{15}N dimension between the two spectra is due to the difference of points collected along this dimension.

4.8 and 50 °C, the optimal experimental conditions determined empirically for NMR study. The buffer used for ultracentrifugation is similar to that for NMR. Since the temperature in the ultracentrifuge can only reach 40 °C, it was not possible to measure homo-oligomerization at 50 °C. Instead, measurements were carried out at three lower temperatures (20, 30, and 40 °C). The monomer−trimer scheme fit the data very well at all three temperatures; the fit for 40 °C is shown in Figure 2A.

The van't Hoff plot of the negative log of the dissociation constants, pK_d, vs 1/T was linear between 20 and 40 °C, indicating that the heat capacity change was negligible (Figure 2B). Assuming that this linear dependence can be extrapolated to higher temperatures, a pK_d of 3.55 in molar fraction units was calculated for 50 °C. On the basis of this value, it can be predicted that >95% of the β3 TM-CYTO protein will be monomeric when the protein/DPC molar ratio is lower than 1/500.

Unlike water-soluble globular proteins, the oligomeric state of membrane proteins does not depend solely on the absolute protein concentration but depends, to a large extent, on the molar ratio of protein and detergent (or lipid). Thus, although the protein concentration used in the ultracentrifugation experiments was 2 orders of magnitude less than that in the NMR experiments, the β3 TM-CYTO protein should remain in the same oligomeric state if the protein/DPC ratio is the same in both experiments. Consistent with this assumption, ^{15}N-HSQC NMR spectra revealed only one protein species, presumably a β3 TM-CYTO monomer, that was detectable when the protein/DPC ratio was ≈1/550. Under these conditions, only two indole cross-peaks were observed in the spectrum, consistent with the presence of two Trp residues in the protein (Figure 2C). When the protein/DPC ratio was increased to approximately 1/200, three major cross-peaks were observed in the same region, consistent with the presence of a significant amount of β3 TM-CYTO trimer. Therefore, all subsequent NMR experiments were carried out at a protein/DPC ratio of 1/550.

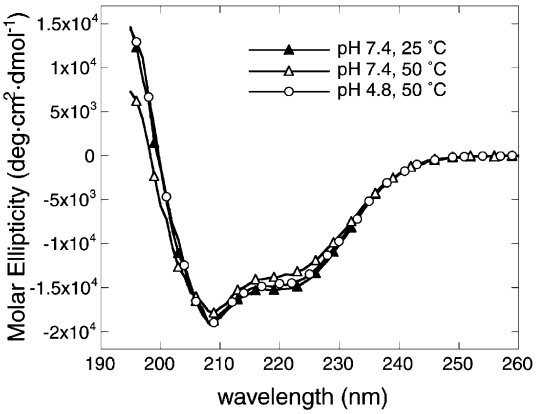

FIGURE 3: CD spectra of the β3 TM-CYTO protein collected at different pH and temperatures.

Temperature and pH Effects on the Protein Conformation. To test whether the conformation of the β3 TM-CYTO protein characterized at pH 4.8 and 50 °C is similar to that under more physiological conditions, CD spectra were collected under various conditions and compared. Figure 3 superimposes three spectra: one taken at pH 4.8 and 50 °C and the other two at pH 7.4 but at 25 and 50 °C. The spectra were similar, all implying a predominant α-helical conforma-

tion. Increasing the temperature from 25 to 50 °C at pH 7.4 produced a small, but reproducible, decrease in molar ellipticity, indicating that the protein was slightly less structured at 50 °C. In contrast, decreasing the pH from 7.4 to 4.8 at 50 °C increased the molar ellipticity values. Coincidentally, the ellipticity increase resulting from the change in pH roughly offsets the decrease from the change in temperature, resulting in nearly identical spectra for pH 4.8, 50 °C and pH 7.4, 25 °C. Thus, it appears that although lowering the pH and raising the temperature affect the overall structure of the β3 TM-CYTO protein, the effects are small and opposite in direction. Accordingly, the conformation of the β3 TM-CYTO protein at pH 4.8 and 50 °C is likely to be a reasonable model for the β3 transmembrane and cytoplasmic domains under physiologic conditions.

Assignment of the β3 TM-CYTO Protein. Assignment of backbone resonances was accomplished mostly using the HNCACB and CBCA(CO)NH experiments (*17*, *18*). Carbonyl carbon chemical shifts were obtained from the HNCO experiment (*19*, *20*). Figure 4A shows ^{15}N strips of HNCACB and CBCA(CO)NH spectra, demonstrating sequential assignments of residues A737−N743. Difficulty in assignment stemmed largely from cross-peak overlap, as well as relatively low signal intensities in the transmembrane domain and the membrane-proximal region of the cytoplasmic tail (Figure 5A). The presence of four Leu-Leu pairs (three are in the transmembrane domain, one in the membrane-proximal region) is noteworthy. Given their locations, these Leu residues would be expected to assume an α-helical conformation. Thus, it is not surprising that many of their C_α and C_β atoms have nearly identical chemical shifts. To resolve the resulting ambiguities, $d_{NN}(i, i+1)$ NOEs were used to define the sequential connectivity (data not shown). Except for the C_β atoms and a few H_β atoms, we could not assign the other side chain atoms.

Figure 4B shows the ^{15}N-HSQC spectrum annotated with resonance assignments. The first two residues do not show cross-peaks in the spectrum, presumably due to the elevated hydrogen exchange rates. Four residues (A-1, K689, G690, and D692), flanking two proline residues (P688 and P691) and all located before the transmembrane region, have two cross-peaks (one major, one minor) in the ^{15}N-HSQC spectrum. We were able to assign these minor peaks through the similar, sometimes identical, C_α and C_β chemical shifts correlated to the same and preceding residue. The characteristic C_α and C_β chemical shifts of the proline residue were also useful. This suggests that the amino terminus of the protein samples at least two conformations. The exchange between these two conformations is slow on the NMR time scale and likely results from proline isomerization.

In contrast to the amino-terminal residues, only one cross-peak was observed for each amide proton in the transmembrane and cytoplasmic domains. The chemical shift dispersion of these amide protons was rather limited. The most upfield HN chemical shift was 7.8 ppm (for T762), and the most downfield was 9.0 ppm (for W715). Such a limited dispersion is consistent with a predominantly α-helical conformation, although some of the cross-peaks are clustered and reminiscent of random coil conformations.

Structure and Dynamics of the β3 TM-CYTO Protein. The secondary structure profile of the protein was generated from chemical shifts using two algorithms implemented in the programs CSI (*26*, *27*) and PSSI (*28*). The C_α, C_β, C′, and H_α chemical shifts, referenced to DSS, were used directly without temperature adjustment. Both programs generated very similar predictions of the secondary structure. Figure 5B plots the probability-based prediction from the program PSSI. The β3 TM-CYTO protein is dominated by an

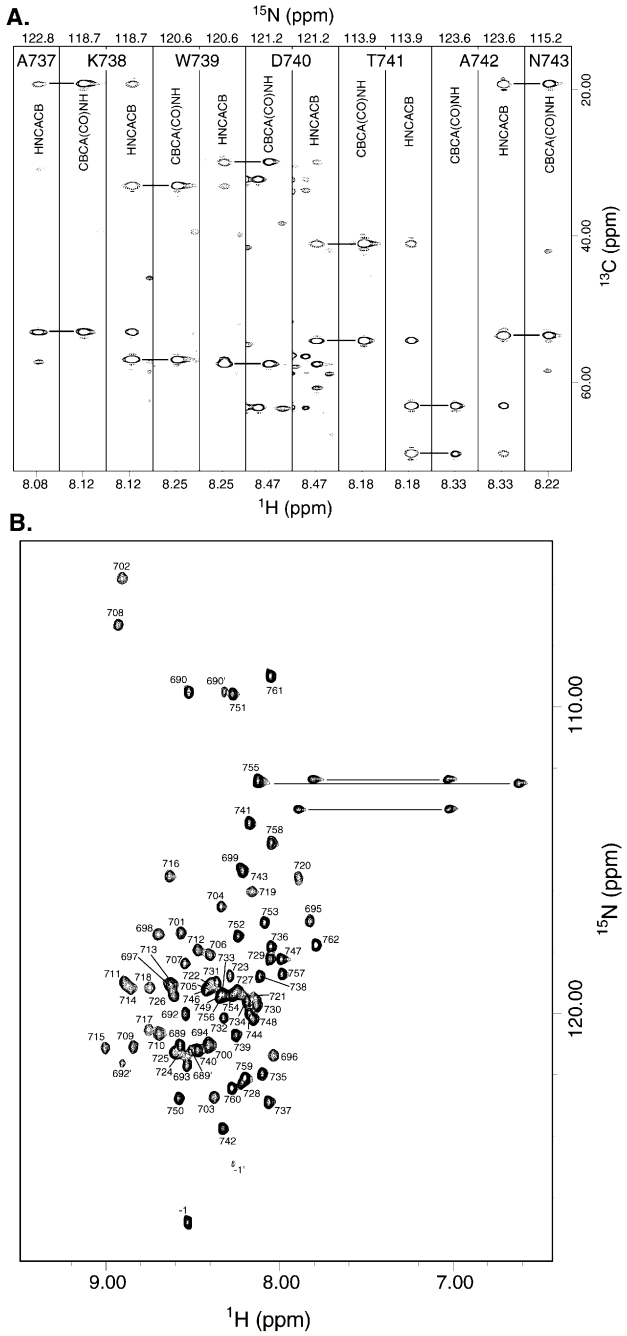

FIGURE 4: Backbone assignment of the β3 TM-CYTO protein. (A) 2D ^{15}N strip plots of the 3D HNCACB and CBCA(CO)NH spectra illustrating the sequential assignment of residues A737−N743. The ^{15}N chemical shift for each strip is indicated on top. Each strip is labeled with the type of spectrum, along with the residue number. Horizontal bars across the strips indicate the connectivity of Cα and Cβ chemical shifts between the residues. (B) 2D ^{15}N-HSQC spectrum of the β3 TM-CYTO protein. The cross-peaks for amide protons are labeled with the residue numbers. The minor peaks of the N-terminal residues are indicated additionally with a prime mark (e.g., 689′). The two cross-peaks from the indole group of Trp residues are not shown here (see Figure 2C). Three solid lines connect the pairs of cross-peaks for Asn N_δ protons.

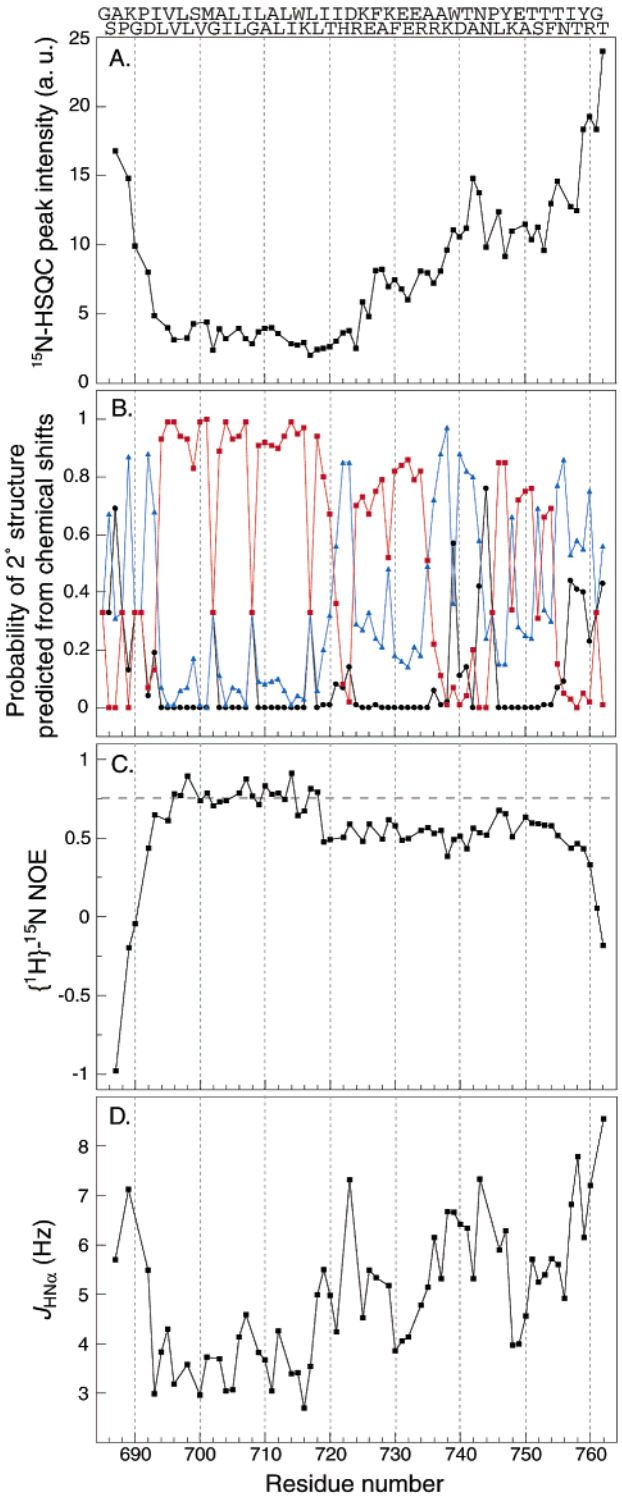

FIGURE 5: NMR-measured structural and dynamic properties for the backbone of the β3 TM-CYTO protein plotted as a function of residue numbers. The protein sequence is shown, in zigzag, on the top. Values for some residues were not obtained due to spectral overlap. (A) Intensities of cross-peaks in the ^{15}N-HSQC spectrum. Signal intensities in other spectra are similar. (B) Probability of secondary structures predicted from combined chemical shifts (*28*). Three types of secondary structure are plotted here: helix (red square), strand (black circle), and coil (blue triangle). The consensus chemical shift index calculated from program CSI (*26*) is very similar and not shown. (C) Heteronuclear {^{1}H}-^{15}N NOE values. The horizontal dashed line indicates the average NOE value for the transmembrane α-helix. (D) $^3J_{HN\alpha}$ coupling constants measured from the HNHA experiment. The error in measurement was approximately 0.5 Hz.

α-helical conformation with very little predicted β-structure. The amino-terminal eight residues are largely random coil, followed by an α-helical transmembrane domain. This helix extends to I721, well past the WK membrane interface motif and through most of the conserved membrane-proximal region. Two stretches in the cytoplasmic tail, K725−A735 and K748−T755, also adopt significant helical secondary structure, albeit with probabilities lower than those for the transmembrane domain. The remainder of the cytoplasmic domain is largely unstructured.

Heteronuclear NOE and $^3J_{HN\alpha}$ coupling constants were measured to obtain a more quantitative view of the protein backbone dynamics (Figure 5C,D). The {^{1}H}-^{15}N NOE value measured for each amide bond reflects the movements of the bond vector on the fast time scale (*22*). A positive NOE value indicates more structured regions. The $^3J_{HN\alpha}$ coupling constant reports the dihedral torsion angle ϕ and smaller values are typical for α-helical conformations (*29*). In the β3 TM-CYTO protein, the transmembrane region could be viewed as an "internal control", as it is expected to take on a stable α-helical conformation in the micelle. As expected, the transmembrane domain (I693−W715) had an average NOE value of 0.77, and most residues in this region had $^3J_{HN\alpha}$ coupling constants between 3 and 4. In contrast, the residues in both termini had low, and sometimes even negative, NOE values and relatively high coupling constants of ∼7 Hz, indicating that both termini are not structured. Measurements were not made for the minor peaks of the N-terminal residues because of low signal-to-noise ratios.

The cytoplasmic residues have lower NOE values than those in the transmembrane domain. Interestingly, most residues, excluding the few carboxyl-terminal ones, maintain a rather uniform NOE value (Figure 5C). The average value for residues I719−T755 is 0.54, much higher than would be expected for a flexible random-coil conformation and only slightly lower than what is expected for a stable rigid structure. This uniformity of the relatively high NOE values suggests that the membrane-distal region of the cytoplasmic domain is largely structured and tumbles as a single structural unit. These results are different from earlier NMR measurements of a construct in which the β3 cytoplasmic tail was fused to a two-stranded helical coiled coil in aqueous solution. In that construct, the highest NOE value was approximately 0.2, and more than half of the residues reported negative values (*14*). The lack of a stable conformation may be due to the insertion of three glycine residues between the coiled-coil sequence and the β3 cytoplasmic tail or the absence of phospholipids or their micellar mimics.

A sharp change in NOE values, rather than a gradual decline, was observed between the transmembrane and cytoplasmic domains. However, the change did not take place at the consensus border between the two domains (Figure 5C). Instead, it was within the membrane-proximal region, between residues L718 and I719. Consistent with the heteronuclear NOE values, the coupling constants increased within the membrane-proximal region to values around 5 Hz, up from 3−4 Hz observed in the transmembrane region. This reflects increased motion in the α-helix extending from the transmembrane domain and is possibly due to fraying near the end of the helix. The helix abruptly ends at the end of the membrane-proximal region. The coupling constant of residue D723 was ∼7 Hz, much higher than those of

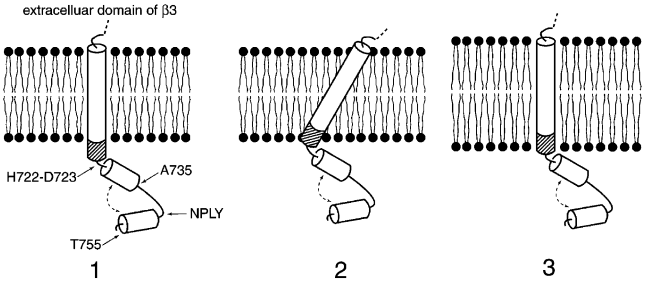

FIGURE 6: Structural model for the transmembrane and cytoplasmic domains of the integrin β3 subunit. The helices are shown as cylinders. Three possible scenarios of the transmembrane helix in the membrane are numbered according to the text. The membrane-proximal region is marked as striped. In the membrane-distal region, the double-headed arrow indicates the possible interactions between the helices.

neighboring residues (Figure 5D). Thus, the HD dipeptide sequence forms a hinge between the membrane-proximal region and the membrane-distal region. Overall, the distal region has higher coupling constants than the transmembrane domain, implying that it is more extended and/or averaged than the latter. Moreover, coupling constants of residues K725−R735 and K748−F754 were around 5 Hz, suggesting that these two regions sample significant α-helical conformation. Therefore, the $^3J_{HN\alpha}$ coupling constants identified the same α-helical regions as predicted from the chemical shift information.

Backbone ^{1}H−^{1}H NOEs also support the conclusion that the protein is primarily α-helical, although the analysis was limited by the degeneracy of the H_N and H_α chemical shifts (see Supporting Information). No $d_{NN}(i, i + 1)$ NOEs were observed for either terminal residues. In contrast, numerous $d_{NN}(i, i + 1)$ NOEs were observed, most of which were in the regions that are α-helical by other indicators. It should be noted that the $d_{NN}(i, i + 1)$ NOE was not observed for residue D723, despite the observation that the H_N chemical shifts of D723 and R724 were sufficiently different. Consistent with the presence of a type I β-turn at the NPLY motif (*14*), the $d_{NN}(i, i + 1)$ NOE of residue L62 was one of the strongest ones. Most of the identified helical-specific $d_{\alpha N}(i, i + 3)$ NOEs were located in the transmembrane domain. In the membrane-proximal region, the only observed $d_{\alpha N}(i, i + 3)$ NOE was between residues W715 and L718, consistent with fraying at the last turn of the helix. In addition, three consecutive $d_{\alpha N}(i, i + 3)$ NOEs were observed for residues A728−F730, confirming that this region is mostly α-helical. Due to spectral overlap, it was impossible to observe any $d_{\alpha N}(i, i + 3)$ NOEs for residues K748−T755.

DISCUSSION

We have characterized the monomeric form of the β3 TM-CYTO protein by NMR spectroscopy. We found that the transmembrane helix extends into the conserved membrane-proximal region of the cytoplasmic domain and ends at approximately H722−D723, consistent with previous glycosylation mapping results (*6*). Thus, it is unlikely that the length of the entire transmembrane helix matches the width of a typical membrane bilayer. There are three possible arrangements for the β3 transmembrane helix with respect to cellular membranes (Figure 6). In the first, the transmembrane helix is oriented in the membrane in an upright fashion and with the membrane-proximal region extending out into the cytoplasm, because the WK sequence is known to favor the membrane interface. In the second, the entire transmembrane helix resides in the membrane but at an angle to accommodate its length, and the membrane-proximal region is shielded from potential binding partners in the cytoplasm. Given the hydrophobic nature of the membrane-proximal region, transition from the first arrangement to the second, and vice versa, would not be energetically costly. Indeed, it has been proposed that movement of the membrane-proximal region in and out of the membrane provides a venue for integrin signaling (*6*, *8*). In the third, the entire transmembrane helix is buried upright in the membrane with increased membrane thickness and a change in its lipid composition. There have been reports that lipid can affect integrin signaling (*30*). Thus, such a movement might provide a possibility for lipid regulation of integrin function.

In contrast to earlier reports (*11*−*14*, *16*), we also observed substantial stable α-helix in the membrane-distal region of the cytoplasmic domain. The cytoplasmic domain, exposed in aqueous solutions but attached at one end to the relatively large micelle complex, would likely have more local fluctuation, and therefore a slightly lower NOE value, than the transmembrane helix that is buried in the micelle. Further, the uniformity of heteronuclear NOE values for most of the β3 cytoplasmic tail suggests that, instead of residing in an extended arrangement, the tail might pack onto itself and behave as a structured domain (Figure 6). Consistent with this possibility, several proteins bind to residues in both the proximal and distal cytoplasmic domain helices, implying that they are in proximity in three-dimensional space (*31*). Our results also suggest that the attachment to the native transmembrane helix and/or the presence of an anisotropic phospholipid−water interface are important for inducing a structured conformation of the β3 tail. This appears to be true for the αIIb counterpart as well, since the isolated αIIb cytoplasmic tail is unstructured in aqueous solutions (*14*) but gains significant α-helical conformation in the presence of trifluoroethanol (*32*). Moreover, when myristoylated at its amino terminus and attached to a DPC micelle, the peptide adopts a well-defined, mostly helical structure (*33*).

Two tyrosine residues are present in the β3 cytoplasmic tail whose phosphorylation state may affect αIIbβ3 function (*34*, *35*). Their separation is similar to that of tyrosines in an immunoreceptor tyrosine-based activation motif (ITAM) present in many cell surface receptors. The sequence NPLY, containing the first tyrosine residue (Y747) that is conserved in many integrin β subunits, has been suggested to induce a type I β-turn and appears to play a role in integrin regulation (*14*, *36*). Our data are consistent with this possibility. Moreover, we found that most of the residues between the tyrosine residues, in particular K748−T755, sample significant α-helical conformation. Such a turn−helix conformation is similar to that of ITAM in the CD3-ϵ CYTO domain (*37*) and may be important for function in general. Moreover, a Y747A mutation, which has been shown to disrupt the turn conformation, inhibits the interaction between talin and the β3 cytoplasmic tail (*14*). Similarly, we propose that the mutation S752P, a naturally occurring mutation that interrupts αIIbβ3-mediated bidirectional signaling pathways in the cell (*38*) and causes Glanzmann thrombasthenia (*39*), may interrupt the important interaction between the β3 cyto-

plasmic tail and interacting proteins by disrupting the helical conformation following the β-turn. It is noteworthy that the introduction of alanine at this position, an amino acid with a helix-forming propensity, does little to alter αIIbβ3 function (*40*).

ACKNOWLEDGMENT

We thank Drs. James Kranz and Peter Flynn for helpful discussion.

SUPPORTING INFORMATION AVAILABLE

One table giving assigned backbone chemical shifts and NOEs of the β3 TM-CYTO protein. This material is available free of charge via the Internet at http://pubs.acs.org.

REFERENCES

1. Hynes, R. O. (1992) *Cell 69*, 11−25.
2. Xiong, J.-P., Stehle, T., Diefenbach, B., Zhang, R., Dunker, R., Scott, D. L., Joachimiak, A., Goodman, S. L., and Arnaout, M. A. (2001) *Science 294*, 339−345.
3. Xiong, J.-P., Stehle, T., Zhang, R., Joachimiak, A., Frech, M., Goodman, S. L., and Arnaout, M. A. (2002) *Science 296*, 151−155.
4. Li, R., Babu, C. R., Lear, J. D., Wand, A. J., Bennett, J. S., and DeGrado, W. F. (2001) *Proc. Natl. Acad. Sci. U.S.A. 98*, 12462−12467.
5. Li, R., Gratowski, H., Mitra, N., Vilaire, G., Lear, J. D., Bennett, J. S., and DeGrado, W. F. (2002) (submitted for publication).
6. Armulik, A., Nilsson, I., von Heijne, G., and Johansson, S. (1999) *J. Biol. Chem. 274*, 37030−37034.
7. Schaller, M. D., Otey, C. A., Hildebrand, J. D., and Parsons, J. T. (1995) *J. Cell Biol. 130*, 1181−1187.
8. Woodside, D. G., Liu, S., and Ginsberg, M. H. (2001) *Thromb. Haemostasis 86*, 316−323.
9. Reszka, A. A., Hayashi, Y., and Horwitz, A. F. (1992) *J. Cell Biol. 117*, 1321−1330.
10. Kaapa, A., Peter, K., and Ylanne, J. (1999) *Exp. Cell Res. 250*, 524−534.
11. Haas, T. A., and Plow, E. F. (1997) *Protein Eng. 10*, 1395−1405.
12. Haas, T. A., and Plow, E. F. (1996) *J. Biol. Chem. 271*, 6017−6026.
13. Muir, T. W., Williams, M. J., Ginsberg, M. H., and Kent, S. B. (1994) *Biochemistry 33*, 7701−7708.
14. Ulmer, T. S., Yaspan, B., Ginsberg, M. H., and Campbell, I. D. (2001) *Biochemistry 40*, 7498−7508.
15. Weljie, A. M., Hwang, P. M., and Vogel, H. J. (2002) *Proc. Natl. Acad. Sci. U.S.A. 99*, 5878−5883.
16. Vinogradova, O., Velyvis, A., Velyviene, A., Hu, B., Haas, T. A., Plow, E. F., and Qin, J. (2002) *Cell 110*, 587−597.
17. Grzesiek, S., and Bax, A. (1993) *J. Biomol. NMR 3*, 185−204.
18. Grzesiek, S., and Bax, A. (1992) *J. Magn. Reson. 99*, 201−207.
19. Ikura, M., Kay, L. E., and Bax, A. (1990) *Biochemistry 29*, 4659−4667.
20. Clubb, R. T., Thanabal, V., and Wagner, G. (1992) *J. Magn. Reson. 97*, 213−217.
21. Marion, D., Kay, L. E., Sparks, S. W., Torchia, D. A., and Bax, A. (1989) *J. Am. Chem. Soc. 111*, 1515−1517.
22. Kay, L. E., Torchia, D. A., and Bax, A. (1989) *Biochemistry 28*, 8972−8979.
23. Vuister, G. W., and Bax, A. (1993) *J. Am. Chem. Soc. 115*, 7772−7777.
24. Delaglio, F., Grzesiek, S., Vuister, G. W., Zhu, G., Pfeifer, J., and Bax, A. (1995) *J. Biomol. NMR 6*, 277−293.
25. Bartels, C., Xia, T., Billeter, M., Guntert, P., and Wüthrich, K. (1995) *J. Biomol. NMR 6*, 1−10.
26. Wishart, D. S., and Sykes, B. D. (1994) *J. Biomol. NMR 4*, 171−180.
27. Wishart, D. S., Bigam, C. G., Holm, A., Hodges, R. S., and Sykes, B. D. (1995) *J. Biomol. NMR 5*, 67−81.
28. Wang, Y., and Jardetzky, O. (2002) *Protein Sci. 11*, 852−861.
29. Case, D. A. (2000) *Curr. Opin. Struct. Biol. 10*, 197−203.
30. Pande, G. (2000) *Curr. Opin. Cell Biol. 12*, 569−574.
31. Patil, S., Jedsadayanmata, A., Wencel-Drake, J. D., Wang, W., Knezevic, I., and Lam, S. C. (1999) *J. Biol. Chem. 274*, 28575−28583.
32. Hwang, P. M., and Vogel, H. J. (2000) *J. Mol. Recognit. 13*, 83−92.
33. Vinogradova, O., Haas, T., Plow, E. F., and Qin, J. (2000) *Proc. Natl. Acad. Sci. U.S.A. 97*, 1450−1455.
34. Law, D. A., DeGuzman, F. R., Heiser, P., Ministri-Madrid, K., Killeen, N., and Phillips, D. R. (1999) *Nature 401*, 808−811.
35. Phillips, D. R., Nannizzi-Alaimo, L., and Prasad, K. S. (2001) *Thromb. Haemostasis 86*, 246−258.
36. O'Toole, T. E., Ylanne, J., and Culley, B. M. (1995) *J. Biol. Chem. 270*, 8553−8558.
37. Borroto, A., Jimenez, M. A., Alarcon, B., and Rico, M. (1997) *Biopolymers 42*, 75−88.
38. Chen, Y. P., O'Toole, T. E., Ylanne, J., Rosa, J. P., and Ginsberg, M. H. (1994) *Blood 84*, 1857−1865.
39. Chen, Y. P., Djaffar, I., Pidard, D., Steiner, B., Cieutat, A. M., Caen, J. P., and Rosa, J. P. (1992) *Proc. Natl. Acad. Sci. U.S.A. 89*, 10169−10173.
40. Ylanne, J., Huuskonen, J., O'Toole, T. E., Ginsberg, M. H., Virtanen, I., and Gahmberg, C. G. (1995) *J. Biol. Chem. 270*, 9550−9557.

BI026822L